Eur. Phys. J. C (2015) 75:23
DOI 10.1140/epjc/s10052-014-3231-6

THE EUROPEAN PHYSICAL JOURNAL C

Regular Article - Experimental Physics

Measurement of the production and lepton charge asymmetry of W bosons in Pb+Pb collisions at $\sqrt{s_{\mathrm{NN}}} = 2.76$ TeV with the ATLAS detector

ATLAS Collaboration[⋆]

CERN, 1211 Geneva 23, Switzerland

Received: 21 August 2014 / Accepted: 15 December 2014 / Published online: 22 January 2015

Abstract A measurement of W boson production in lead-lead collisions at $\sqrt{s_{\mathrm{NN}}} = 2.76$ TeV is presented. It is based on the analysis of data collected with the ATLAS detector at the LHC in 2011 corresponding to an integrated luminosity of 0.14 nb^{-1} and 0.15 nb^{-1} in the muon and electron decay channels, respectively. The differential production yields and lepton charge asymmetry are each measured as a function of the average number of participating nucleons $\langle N_{\mathrm{part}} \rangle$ and absolute pseudorapidity of the charged lepton. The results are compared to predictions based on next-to-leading-order QCD calculations. These measurements are, in principle, sensitive to possible nuclear modifications to the parton distribution functions and also provide information on scaling of W boson production in multi-nucleon systems.

1 Introduction

Studies of particle production in the high-density medium created in ultra-relativistic heavy-ion collisions have been previously conducted at the Relativistic Heavy Ion Collider (RHIC) at Brookhaven National Laboratory [1–4] and have been extended to larger centre-of-mass energies at the Large Hadron Collider (LHC) at CERN [5,6]. These collisions provide access to a phase of nuclear matter at high temperature and low baryon density called quark–gluon plasma (QGP), in which the relevant degrees of freedom are quarks and gluons [7–11]. In a QGP, high-energy partons transfer energy to the medium through multiple interactions and gluon radiation, resulting in a modification of the parton shower of jets (jet-quenching). This effect is consistent with the measurements of high transverse momentum (p_{T}) charged hadron yields [12–16], inclusive jets [17] and dijets with asymmetric transverse energies (E_{T}) [18–20].

Electroweak bosons ($V = \gamma, W, Z$) provide additional ways to study partonic energy loss in heavy-ion collisions. They do not interact strongly with the medium, thus offering a means to calibrate the energy of jets in V-jet events. At sub-TeV centre-of-mass energies, the only viable candidates for playing this role are photons [21]. However at higher energies, heavy gauge bosons ($W^{\pm}$ and Z) are also produced in relatively high abundance, introducing an additional avenue for benchmarking in-medium modifications to coloured probes. This potential has already been realised in lead–lead (Pb+Pb) collisions in previous ATLAS [22] and CMS [23–25] publications, where it was observed that electroweak boson production rates scale linearly with the number of binary nucleon–nucleon collisions.

Moreover, in principle, electroweak bosons are an excellent tool for studying modifications to parton distribution functions (PDFs) in a multi-nucleon environment. To leading-order, $W^+(W^-)$ bosons are primarily produced by interactions between a $u(d)$ valence quark and a $\overline{d}(\overline{u})$ sea quark. The rapidity of the W boson is primarily determined by the momentum fractions, x, of the incoming partons. Therefore, information about the PDF can be extracted by measuring the charge asymmetry as a function of the pseudorapidity[1] of charged leptons produced from W decays.

The charge asymmetry is defined in terms of the differential production yields for $W \to \ell\nu_\ell$ ($\ell = \mu, e$), $\mathrm{d}N_{W\to\ell\nu_\ell}/\mathrm{d}\eta_\ell$:

$$A_\ell(\eta_\ell) = \frac{\mathrm{d}N_{W^+\to\ell^+\nu_\ell}/\mathrm{d}\eta_\ell - \mathrm{d}N_{W^-\to\ell^-\bar{\nu}_\ell}/\mathrm{d}\eta_\ell}{\mathrm{d}N_{W^+\to\ell^+\nu_\ell}/\mathrm{d}\eta_\ell + \mathrm{d}N_{W^-\to\ell^-\bar{\nu}_\ell}/\mathrm{d}\eta_\ell} \tag{1}$$

where η_ℓ is the pseudorapidity of the charged lepton and the W boson production yields are determined in the kinematic

⋆ e-mail: atlas.publications@cern.ch

[1] The ATLAS detector uses a right-handed coordinate system with the nominal Pb+Pb interaction point at its centre. The z-axis is along the beam pipe. The x-axis points from the interaction point toward the centre of the ring and the y-axis points upward. Cylindrical coordinates (r, ϕ) are used in the transverse plane with ϕ being the azimuthal angle around the z-axis. The pseudorapidity is defined in terms of the polar angle θ as $\eta = -\ln(\tan\theta/2)$.

phase space used to select $W \to \ell\nu_\ell$ events. This observable has been used to study PDFs in binary nucleon systems such as pp collisions at the LHC [26–28] and $p\bar{p}$ collisions at the Tevatron [29,30]. However, its utility in nuclear systems has only recently been explored with a limited set of experimental data [25].

Although the method for measuring the charge asymmetry in Pb+Pb is essentially identical to that in pp, the distributions themselves are not expected to be identical. In pp collisions, the overall production rate of W^+ bosons is larger than that of W^- bosons as a result of the larger fraction of u valence quarks relative to d valence quarks in the colliding system. On the other hand, in Pb+Pb collisions, the nuclei contain 126 neutrons and 82 protons. Thus, pp interactions make up only ≈15 % of the total number of nucleon–nucleon interactions, whereas neutron–neutron (nn) and proton–neutron (pn) combinations contribute ≈37 % and ≈48 %, respectively. Consequently, a marked difference is expected in the lepton charge asymmetry between Pb+Pb and pp collisions.

Prior to this analysis, the only published charge asymmetry measurement in heavy-ion collisions was reported by the CMS collaboration [25] with an integrated luminosity of 7.3 μb^{-1} using the $W \to \mu\nu_\mu$ channel in Pb+Pb collisions at $\sqrt{s_{\text{NN}}} = 2.76$ TeV. The measurement presented here uses a dataset from 2011, which corresponds to an integrated luminosity of 0.14 and 0.15 nb^{-1} for the muon and electron channels, respectively. In addition, the $W \to e\nu_e$ decay mode is employed for the first time in a heavy-ion environment.

The paper is organised as follows: a brief overview of the ATLAS detector and trigger is given in Sect. 2. A description of the simulated event samples used in the analysis is provided in Sect. 3. The criteria for selecting Pb+Pb events are presented in Sect. 4. This is followed by a description of muon and electron reconstruction and signal candidate selection in Sect. 5. The background estimations are presented in Sect. 6. A discussion of the procedure for correcting the signal yields is presented in Sect. 7. The systematic uncertainties and the combination of the two channels are described in Sect. 8, and the W boson production yields, measured as a function of the mean number of inelastically interacting nucleons $\langle N_{\text{part}} \rangle$ and $|\eta_\ell|$, are discussed in Sect. 9. A differential measurement of the lepton charge asymmetry as a function of $|\eta_\ell|$ is also presented. These results are compared to predictions at next-to-leading order (NLO) [31–33] in QCD, both with and without nuclear corrections. The former is represented by the EPS09 PDF [34]. Section 10 provides a brief summary of the results.

2 The ATLAS detector

ATLAS [35], one of four large LHC experiments, is well equipped to carry out an extensive heavy-ion program. The inner detector (ID) comprises a precision tracking system that covers a pseudorapidity range $|\eta| < 2.5$. The ID consists of silicon pixels, silicon microstrips, and a transition radiation tracker (TRT)[2] consisting of cylindrical drift tubes and operates within a 2 T axial magnetic field supplied by a superconducting solenoid.

Due to the high occupancy in heavy-ion events, tracks of charged particles are reconstructed using only the silicon pixels and microstrips. No information from the TRT is used in this analysis, and henceforth ID tracks will refer to those tracks that are reconstructed without this detector component.

Outside the solenoid, highly segmented electromagnetic (EM) and hadronic sampling calorimeters cover the region $|\eta| < 4.9$. The EM calorimetry is based on liquid-argon (LAr) technology and is divided into one barrel ($|\eta| < 1.475$, EMB) and two end-cap ($1.375 < |\eta| < 3.2$, EMEC) components. The transition region between the barrel and end-cap calorimeters is located within the pseudorapidity range $1.37 < |\eta| < 1.52$. The hadronic calorimeter is based on two different detector technologies: steel absorber interleaved with plastic scintillator covering the barrel ($|\eta| < 1.0$) and extended barrels ($0.8 < |\eta| < 1.7$) and LAr hadronic end-cap calorimeters (HEC) located in the region $1.5 < |\eta| < 3.2$. A forward calorimeter (FCal) that uses LAr as the active material is located in the region $3.1 < |\eta| < 4.9$. On the inner face of the end-cap calorimeter cryostats, a minimum-bias trigger scintillator (MBTS) is installed on each side of the ATLAS detector, covering the pseudorapidity region $2.1 < |\eta| < 3.8$.

The outermost sub-system of the detector is a muon spectrometer (MS) that is divided into a barrel region ($|\eta| < 1.05$) and two end-cap regions ($1.05 < |\eta| < 2.7$). Precision measurements of the track coordinates and momenta are provided by monitored drift tubes (MDTs), cathode strip chambers (CSCs), and three sets of air-core superconducting toroids with coils arranged in an eight-fold symmetry that provide on average 0.5 T in the azimuthal plane.

The zero-degree calorimeters (ZDCs) [36] are located symmetrically at $z = \pm 140$ m and cover $|\eta| > 8.3$. In Pb+Pb collisions the ZDCs primarily measure spectator neutrons from the colliding nuclei.

The ATLAS detector also includes a three-level trigger system [37]: level one (L1) and the software-based High Level Trigger (HLT), which is subdivided into the Level 2 (L2) trigger and Event Filter (EF). Muon and electron triggers are used to acquire the data analysed in this paper.

The trigger selection for muons is performed in three steps. Information is provided to the L1 trigger system by the fast-response resistive plate chambers (RPCs) in the barrel ($|\eta| < 1.05$) and thin gap chambers (TGCs) in the end-caps ($1.05 < |\eta| < 2.4$). Both the RPCs and TGCs are part

[2] The TRT provides tracking information up to $|\eta| < 2$.

of the MS. Information from L1 is then passed to the HLT, which reconstructs muon tracks in the vicinity of the detector region reported by the L1 trigger. The L2 trigger performs a fast reconstruction of muons using a simple algorithm, which is then further refined at the EF by utilising the full detector information as in the offline muon reconstruction software.

The trigger selection for electrons is performed using a L1 decision based on electromagnetic energy depositions in trigger towers of $\Delta\phi \times \Delta\eta = 0.1 \times 0.1$ formed by EM calorimeter cells within the range $|\eta| < 2.5$. The electron trigger algorithm identifies a region of interest as a trigger tower cluster for which the transverse energy (E_{T}) sum from at least one of the four possible pairs of nearest neighbour towers exceeds a specified E_{T} threshold.

3 Monte Carlo samples

Simulated event samples are produced using the Monte Carlo (MC) method and are used to estimate both the signal and background components. The response of the ATLAS detector is simulated using GEANT4 [38,39]. The samples used throughout this paper are summarised in Table 1. Each signal process and most of the background processes are embedded into minimum-bias (MB) heavy-ion events from data recorded in the same run periods as the data used to analyse W boson production. Events from the $Z \to \mu^+\mu^-$ channel are embedded into HIJING [40] – a widely used heavy-ion simulation that reproduces many features of the underlying event [17].

The production of W bosons and its decay products are modelled with the POWHEG [41] event generator, which is interfaced to PYTHIA8 [42] in order to model parton showering and fragmentation processes. These samples use the CT10 [43] PDF set and are used to estimate the signal selection efficiency and to provide predictions from theory. In order to account for the isospin of the nucleons, separate samples of pp, pn, and nn events are generated and combined in proportion to their corresponding collision frequency in Pb+Pb collisions. Only pp simulations are used to model background processes (discussed in detail in Sect. 6) since these channels are not sensitive to isospin effects.

Table 1 Signal and background simulated event samples used in this analysis. $W \to \ell\nu_\ell$ events include all nucleon combinations, whereas background processes use only pp simulations. The variable $\hat{p}_{\mathrm{T}}$ is the average p_{T} of the two outgoing partons involved in the hard-scattering process evaluated before modifications from initial- and final-state radiation. Details for each sample are given in the text

Physics process	Generator	PDF set
$W \to \mu\nu_\mu$	POWHEG+PYTHIA8	CT10
$W \to e\nu_e$	POWHEG+PYTHIA8	CT10
Dijet	PYTHIA6	MRST LO*
($17 < \hat{p}_{\mathrm{T}} < 140$ GeV)		
$Z \to \mu^+\mu^-$	PYTHIA6	MRST LO*
$Z \to e^+e^-$	POWHEG+PYTHIA8	CT10
$W \to \tau\nu_\tau \to \mu\nu_\mu\nu_\tau\nu_\tau$	PYTHIA6	MRST LO*
$W \to \tau\nu_\tau \to e\nu_e\nu_\tau\nu_\tau$	POWHEG+PYTHIA8	CT10

Background samples are generated for muons with PYTHIA6 using the MRST LO* PDF set [44] and for electrons with POWHEG using the CT10 PDF set. At the level of the precision of the background estimation, no significant difference is expected between the PYTHIA6 and POWHEG generators. The background contribution to the muon channel from heavy-flavour is modelled using simulated dijet samples with average final-state parton energies $\hat{p}_{\mathrm{T}}$ in the range 17–140 GeV. Tau decays from $W \to \tau\nu_\tau$ events are treated using either TAUOLA [45] or PYTHIA8 for final states involving muons or electrons, respectively. Final-state radiation from QED processes is simulated by PHOTOS [46].

4 Event selection

4.1 Centrality definition

Pb+Pb collision events are selected by imposing basic requirements on the beam conditions and the performance of each sub-detector. In order to select MB hadronic Pb+Pb collisions, a hit on each side of the MBTS system with a time coincidence within 3 ns is required for each collision. In addition, each event is required to have a reconstructed vertex with at least three associated high-quality tracks [47] compatible with the beam-spot position. These requirements select MB hadronic Pb+Pb collisions in the data with an efficiency of (98 ± 2) % with respect to the total non-Coulombic inelastic cross-section [5]. After accounting for the selection efficiency and prescale factors imposed by the trigger system during data taking [48], approximately 1.03×10^9 Pb+Pb events are sampled (denoted by N_{events} hereafter).

Each event is categorised into a specific centrality class defined by selections on FCal ΣE_{T}, the total transverse energy deposited in the FCal and calibrated to the EM energy scale [47]. Centrality classes in heavy-ion events represent the percentiles of the total inelastic non-Coulombic Pb+Pb cross-section. This reflects the overlap volume between the colliding nuclei and allows for selection of various collision geometries in the initial state.

The FCal ΣE_{T} is closely related to the mean number of inelastically interacting nucleons $\langle N_{\mathrm{part}} \rangle$ and mean number of binary collisions $\langle N_{\mathrm{coll}} \rangle$ through the Glauber formalism [49]. $\langle N_{\mathrm{part}} \rangle$ and $\langle N_{\mathrm{coll}} \rangle$ are monotonic functions of the collision impact parameter and are correlated with the FCal ΣE_{T} of each Pb+Pb collision [5]. $\langle N_{\mathrm{coll}} \rangle$ can also

Table 2 Average number of participating nucleons $\langle N_{\text{part}} \rangle$ and binary collisions $\langle N_{\text{coll}} \rangle$ for the centrality classes used in this analysis alongside their relative uncertainties

Centrality [%]	$\langle N_{\text{part}} \rangle$	$\delta\langle N_{\text{part}} \rangle$ [%]	$\langle N_{\text{coll}} \rangle$	$\delta\langle N_{\text{coll}} \rangle$ [%]
0–5	382	0.5	1683	7.7
5–10	330	0.9	1318	7.5
10–20	261	1.4	923	7.4
20–40	158	2.6	441	7.3
40–80	46	6.0	78	9.4
0–80	140	4.7	452	8.5

be expressed as the product of the average nuclear thickness function $\langle T_{AA} \rangle$ and the total inelastic pp cross-section (64 ± 5 mb at $\sqrt{s} = 2.76$ TeV [50]). In this paper, events are separated into five centrality classes: 0–5 %, 5–10 %, 10–20 %, 20–40 %, and 40–80 % with the most central interval (0–5 %) corresponding to the 5 % of events with the largest FCal ΣE_{T}. The $\langle N_{\text{coll}} \rangle$ estimation in the 80–100 % class suffers from high experimental uncertainties, and therefore, this centrality class is not considered in the analysis. Table 2 presents $\langle N_{\text{part}} \rangle$ and $\langle N_{\text{coll}} \rangle$ for each centrality class along with their relative systematic uncertainties (see Sect. 8). Since a single participant can interact inelastically with several nucleons in a collision, the uncertainty in $\langle N_{\text{part}} \rangle$ is less than that of the corresponding $\langle N_{\text{coll}} \rangle$ in each centrality class.

4.2 Trigger selection

$W \to \mu\nu_\mu$ candidates are selected using single muon triggers with a requirement on the minimum transverse momentum of 10 GeV in the HLT. Two types of single muon triggers are used: one that requires a muon in coincidence with a total event transverse energy – measured in the calorimeter at L1 – above 10 GeV and another which requires a muon in coincidence with a neutral particle at $|\eta| > 8.3$ in the ZDCs. This combination of triggers maximises the efficiency for events across all centrality classes. The muon trigger efficiencies are evaluated using high-quality single muons reconstructed from MB events and range from 89.3 % to 99.6 %, depending on $|\eta_\mu|$ and the centrality of the event from which the muon originated.

Candidate events for $W \to e\nu_e$ are selected using only the hardware-based L1 trigger, i.e. without use of the HLT. The L1 calorimeter trigger selects photon and electron candidates in events where the transverse energy in an EM cluster of trigger towers exceeds 14 GeV. The efficiency is evaluated using a tag-and-probe method that utilises $Z \to e^+e^-$ events selected using the criteria from Ref. [22]. This gives an efficiency of 99.6 % for electrons with $E_{\text{T}} > 25$ GeV and $|\eta| < 2.47$ – excluding the transition region – with a negligible centrality dependence.

4.3 Transverse momentum imbalance, $p_{\text{T}}^{\text{miss}}$

Previous W boson analyses in ATLAS [26] have used the event momentum imbalance in the plane transverse to the beam axis ($E_{\text{T}}^{\text{miss}}$) as a proxy for the true neutrino p_{T}. Traditionally, these analyses reconstruct the $E_{\text{T}}^{\text{miss}}$ using contributions from energy deposits in the calorimeters and muons reconstructed in the MS [51]. In minimum bias events, no genuine missing energy is expected, and the resolution of the two $E_{\text{T}}^{\text{miss}}$ components (σ_x^{miss}, σ_y^{miss}) is measured directly from reconstructed quantities in the data by assuming the true $E_{\text{x}}^{\text{miss}}$ and $E_{\text{y}}^{\text{miss}}$ are zero. The resolution is estimated from the width of the $E_{\text{x}}^{\text{miss}}$ and $E_{\text{y}}^{\text{miss}}$ distributions. In heavy-ion collisions, soft particle production is much higher than in pp collisions, thereby resulting in an increased number of particles that do not reach the calorimeter or seed a topocluster. Consequently, the resolution in the $E_{\text{T}}^{\text{miss}}$ observed in the data using calorimeter cells is at the level of 45 GeV in the most central heavy-ion events. Therefore, this analysis employs a track-based calculation proposed in Ref. [25] that provides a four-fold improvement in resolution relative to the calorimeter-based method. The event momentum imbalance using this approach is defined as the negative vector sum of all high-quality ID tracks [47] with $p_{\text{T}} > 3$ GeV:

$$\mathbf{p}^{\text{miss}} = -\sum_{\text{i}=1}^{N_{\text{tracks}}} \mathbf{p}_{\text{i}}^{\text{track}}, \tag{2}$$

where $\mathbf{p}_{\text{i}}^{\text{track}}$ is the momentum vector of the i^{th} ID track, and N_{tracks} represents the total number of ID tracks in the event. The magnitude of the transverse component $p_{\text{T}}^{\text{miss}}$ and azimuthal angle ϕ^{miss} are calculated from the transverse components ($p_{\text{x}}^{\text{miss}}$ and $p_{\text{y}}^{\text{miss}}$) of the resultant vector. The lower track p_{T} threshold is chosen based on that which gives the best resolution in the $p_{\text{T}}^{\text{miss}}$ while still including a sufficient number of tracks in the vector summation.

The transverse mass of the charged lepton and neutrino system is defined as

$$m_{\text{T}} = \sqrt{2 p_{\text{T}}^{\ell} p_{\text{T}}^{\text{miss}} (1 - \cos \Delta\phi_{\ell, p_{\text{T}}^{\text{miss}}})}, \tag{3}$$

where $\Delta\phi_{\ell, p_{\text{T}}^{\text{miss}}}$ is the difference between the direction of the charged lepton and $p_{\text{T}}^{\text{miss}}$ vector in the azimuthal plane.

5 Signal candidate reconstruction and selection

5.1 Muon reconstruction

Muon reconstruction in ATLAS consists of separate tracking in the ID and MS. In this analysis, tracks reconstructed in each sub-system are combined using the χ^2-minimisation

procedure described in Ref. [52]. These combined muons are required to satisfy selection criteria that closely follow those used in the Z boson analysis in Pb+Pb data [22]. To summarise, these criteria include a set of ID hit requirements in the pixel and SCT layers of the ID, a selection on the transverse and longitudinal impact parameters ($|d_0|$ and $|z_0|$), and a minimum requirement on the quality of the muon track fit. Additional selection criteria specific to W bosons are discussed below.

Decays-in-flight from pions and kaons contribute a small background fraction in this analysis. They are reduced by requiring the difference between the ID and MS muon p_{T} measurements (corrected for the mean energy loss due to interactions with the material between the ID and MS) to be less than 50 % of the p_{T} measured in the ID. Decays-in-flight are further reduced by locating changes in the direction of the muon track trajectory. This is performed using a least-squares track fit that includes scattering angle parameters accounting for multiple scattering between the muon and detector material. Scattering centers are allocated along the muon track trajectory from the ID to MS, and decays are identified by scattering angle measurements much greater than the expectation value due to multiple scattering [53].

In order to reduce the multi-jet contribution, a track-based isolation of the muon is imposed. The tracks are taken from a cone radius $\Delta R = \sqrt{(\Delta\eta)^2 + (\Delta\phi)^2} = 0.2$ around the direction of the muon. The muon is considered isolated if the sum of the transverse momenta of ID tracks ($\sum p_{\mathrm{T}}^{\mathrm{ID}}$) with $p_{\mathrm{T}} > 3$ GeV – excluding the muon p_{T} itself – is less than 10 % of the muon p_{T}. In this paper, the quantity $\sum p_{\mathrm{T}}^{\mathrm{ID}}/p_{\mathrm{T}}$ is referred to as the muon isolation ratio. Based on MC studies, the isolation requirement is estimated to reject 50–70 % of muons in QCD multi-jet events, depending on the centrality class, while retaining at least 95 % of signal candidates.

5.2 Electron reconstruction

In order to reconstruct electrons in the environment of heavy-ion collisions, the energy deposits from soft particle production due to the underlying event (UE) must be subtracted, as they distort calorimeter-based observables. The two-step subtraction procedure, described in detail in Ref. [17], is applied. It involves calculating a per-event average UE energy density that excludes contributions from jets and EM clusters and accounts for effects from elliptic flow modulation on the UE. The residual deposited energies stem primarily from three sources: photons/electrons, jets and UE fluctuations (including higher-order flow harmonics). After the UE background subtraction, a standard ATLAS electron reconstruction and identification algorithm [54,55] for heavy-ions is used – the only difference between this algorithm and the one used in pp collisions is that the TRT is not used. The algorithm is designed to provide various levels of background rejection and high identification efficiencies over the full acceptance of the ID system.

The electron identification selections are based on criteria that use calorimeter and tracking information and are optimised in bins of η and E_{T}. Patterns of energy deposits in the first layer of the EM calorimeter, track quality variables, and a cluster-track matching criterion are used to select electrons. Selection criteria based on shower shape information from the second layer of the EM calorimeter and energy leakage into the hadronic calorimeters are used as well. Background from charged hadrons and secondary electrons from conversions are reduced by imposing a requirement on the ratio of cluster energy to track momentum. Electrons from conversions are further reduced by requiring at least one hit in the first layer of the pixel detector.

A calorimeter-based isolation variable is also imposed. Calorimeter clusters are taken within $\Delta R = 0.25$ around the candidate electron cluster. An electron is considered isolated if the total transverse energy of calorimeter clusters – excluding the candidate electron cluster – is less than 20 % of the electron E_{T}. In this paper, the quantity $\sum E_{\mathrm{T}}^{\mathrm{calo}}/E_{\mathrm{T}}$ is referred to as the electron isolation ratio. The isolation requirement was studied in each centrality class and retains, on average, 92 % of signal candidates while rejecting 42 % of electrons from QCD multi-jet events.

5.3 W boson candidate selection

W boson production yields are measured in a fiducial region defined by:

$$
\begin{aligned}
W \to \mu\nu_\mu: \quad & p_{\mathrm{T}}^{\mu} > 25\ \mathrm{GeV}, \quad 0.1 < |\eta_\mu| < 2.4, \\
& p_{\mathrm{T}}^{\nu} > 25\ \mathrm{GeV}, \quad m_{\mathrm{T}} > 40\ \mathrm{GeV}; \\
W \to e\nu_e: \quad & p_{\mathrm{T}}^{e} > 25\ \mathrm{GeV}, \quad |\eta_e| < 2.47, \\
& \text{excluding } 1.37 < |\eta_e| < 1.52, \\
& p_{\mathrm{T}}^{\nu} > 25\ \mathrm{GeV}, \quad m_{\mathrm{T}} > 40\ \mathrm{GeV}.
\end{aligned}
$$

In the MS, a gap in chamber coverage is located at $|\eta_\mu| < 0.1$ that allows for services to the solenoid magnet, calorimeters, and ID, and therefore, this region is excluded. The most forward bin boundary is determined by the acceptance of the muon trigger chambers. In the electron analysis, the calorimeter transition region at $1.37 < |\eta_e| < 1.52$ is excluded. The lower limit on the m_{T} is imposed to further suppress background events that satisfy the lepton p_{T} and $p_{\mathrm{T}}^{\mathrm{miss}}$ requirements.

In the muon channel, the background contribution from $Z \to \mu^+\mu^-$ decays is suppressed by rejecting muons from opposite-charge pairs that have an invariant mass greater than 66 GeV. These events are selected by requiring that one muon in the pair has $p_{\mathrm{T}} > 25$ GeV and passes the quality requirements in Sect. 5.1 and the other muon in the pair satisfies a lower p_{T} threshold of 20 GeV. In principle, this method allows for the possibility of accepting events with more than

one W boson. However, only one event in the data was found where two muons satisfy all signal selection requirements. This selection vetoes 86 % of muons produced from Z bosons while retaining over 99 % of W boson candidates. The 14 % of background muons that satisfy the selection criteria is attributable to instances where the second muon from the Z boson decay is produced outside the ID acceptance or has $p_{\mathrm{T}} < 20$ GeV.

In the electron channel, the $Z \to e^+e^-$ background contribution is suppressed by rejecting events with more than one electron satisfying the identification requirements from Sect. 5.2. This selection retains over 99 % of signal events while rejecting 23 % of Z boson candidates. Events surviving the selection are attributable to instances where the second electron from the Z boson decay is either produced outside the ID acceptance (26 %) or does not pass the relatively tight electron identification requirements (74 %).

After applying all selection criteria, 3348 W^+ and 3185 W^- candidates are detected in the muon channel. In the electron channel, 2893 W^+ and 2791 W^- candidates are observed.

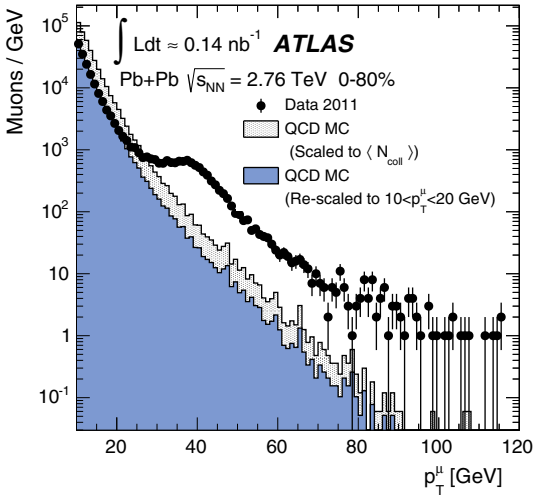

Fig. 1 Muon transverse momentum distribution in the data (*points*) before applying the signal selection requirements. The p_{T} distribution of QCD multi-jet processes from the MC simulation is also shown in the same figure. The *shaded histogram* is scaled to $\langle N_{\mathrm{coll}} \rangle$ and the *solid histogram* is rescaled to match the data in a control region $10 < p_{\mathrm{T}}^{\mu} < 20$ GeV. The background fraction from QCD multi-jet processes is determined from the number of muons in the MC surviving the final selection criteria

6 Background estimation

The main backgrounds to the $W \to \ell\nu_\ell$ channel arise from lepton production in electroweak processes and semileptonic heavy-flavour decays in multi-jet events. The former include $W \to \tau\nu_\tau \to \ell\nu_\ell\nu_\tau\nu_\tau$ events and $Z \to \ell^+\ell^-$ events, where one lepton from the Z boson is emitted outside the ID acceptance and produces spurious $p_{\mathrm{T}}^{\mathrm{miss}}$. Other sources of background that are considered include $Z \to \tau\tau$ events, in which at least one tau decays into a muon or electron, and $t\bar{t}$ events, in which at least one top quark decays semileptonically into a muon or electron. These two background sources are negligible (<0.5 %) and are not taken into account in this analysis.

6.1 $W \to \mu\nu_\mu$ channel

In the muon channel, the total number of background events from QCD multi-jet processes is estimated using a partially data-driven method. The dijet muon yields per Pb+Pb event in the MC simulation are normalised to the pp cross-section and scaled by the number of binary collisions and Pb+Pb events in the data. The resulting distribution is represented by the shaded histogram in Fig. 1. To take into account jet energy-loss in the medium, the MC distribution is rescaled to the data in a control region dominated by QCD multi-jet events in the range $10 < p_{\mathrm{T}}^{\mu} < 20$ GeV (solid histogram). This scale factor is on average 0.4 over all $|\eta_\mu|$ intervals and centrality classes. As a cross-check, the shape of the rescaled QCD multi-jet background distribution was compared to that of a control sample consisting of anti-isolated muons from the data. They are found to agree well, confirming that the distributions in Fig. 1 are an accurate representation of the multi-jet background in the data. The number of expected QCD multi-jet events is determined by extrapolating the rescaled MC distribution from the control region to the signal p_{T}^{μ} region above 25 GeV. The fraction of background events in the data is then calculated from the ratio of the number of QCD multi-jet events surviving final selection in the MC and the number of W candidates in the data. This is performed as function of η_μ and centrality. The background fraction is also determined separately for μ^+ and μ^-, and no charge dependence is observed. The multi-jet background fraction is estimated to be on average 3.7 % of the total number of $W^{\pm}$ boson candidates, varying from 2.0 % to 5.4 % as a function of η_μ and centrality.

The estimated number of background events from electroweak processes is determined separately for the $Z \to \mu^+\mu^-$ and $W \to \tau\nu_\tau$ channels. The background from $Z \to \mu^+\mu^-$ events is determined in each η_μ interval from MC simulation and scaled to reproduce the actual number of $Z \to \mu^+\mu^-$ events observed in the data [22] in each centrality class. This contribution is on average 2.4 % relative to the total number of W boson candidates and ranges from 1.0 % at central $|\eta_\mu|$ to 3.2 % in the forward region. Background events originating from $W \to \tau\nu_\tau \to \mu\nu_\mu\nu_\tau\nu_\tau$ decays are estimated by calculating the ratio of the number of $W \to \tau\nu_\tau \to \mu\nu_\mu\nu_\tau\nu_\tau$ and $W \to \mu\nu_\mu$ events that satisfy the analysis selection in the simulation. This fraction is on average 1.5 % in each $|\eta_\mu|$ interval and centrality class and is applied to the number of observed signal candidates. Variations

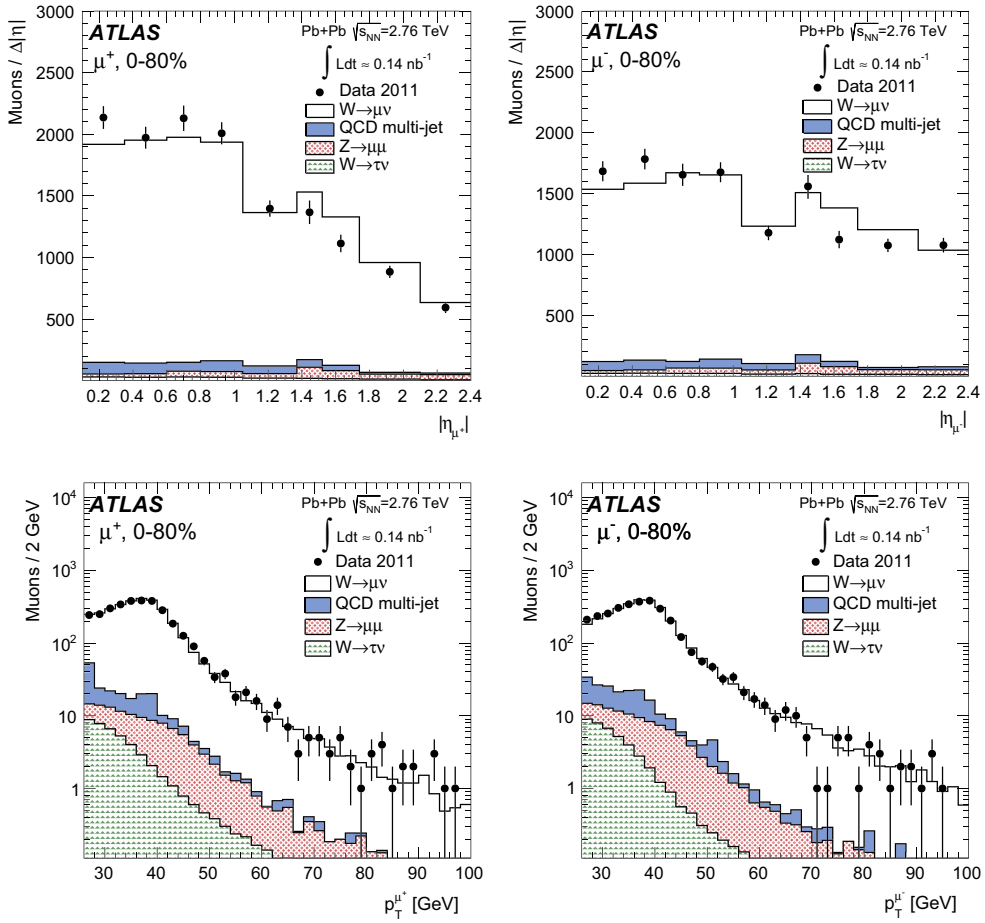

Fig. 2 Measured muon absolute pseudorapidity (*top*) and transverse momentum (*bottom*) distributions for $W^+ \to \mu^+\nu_\mu$ (*left*) and $W^- \to \mu^-\bar{\nu}_\mu$ (*right*) candidates after applying the complete set of selection requirements in the fiducial region, $p_{\mathrm{T}}^{\mu} > 25$ GeV, $p_{\mathrm{T}}^{\mathrm{miss}} > 25$ GeV, $m_{\mathrm{T}} > 40$ GeV and $0.1 < |\eta_\mu| < 2.4$. The contributions from electroweak and QCD multi-jet processes are normalised according to their expected number of events. The $W \to \mu\nu_\mu$ MC events are normalised to the number of background-subtracted events in the data. The background and signal predictions are added sequentially

between bins are at the level of 1.3–1.8 %. The expected background from all sources in the $W \to \mu\nu_\mu$ channel amounts to 7.6 % of the total number of W boson candidates.

Figure 2 shows the $|\eta_\mu|$ and p_{T}^{μ} distributions for positively and negatively charged muons after final event selection. Figure 3 presents the event $p_{\mathrm{T}}^{\mathrm{miss}}$ and m_{T} distributions. In each figure, the data are compared to signal and background distributions from MC simulation in the same phase space. The background distributions are normalised to the expected number of events, whereas the signal MC distribution is normalised to the number of background-subtracted events in the data. The background and signal predictions in Figs. 2 and 3 are added sequentially, beginning with the contribution from $W \to \tau\nu_\tau$.

6.2 $W \to e\nu_e$ channel

A partially data-driven method is used to estimate the QCD multi-jet background observed in $W \to e\nu_e$ candidate events. This method involves using a control sample from the data to construct a QCD background template and simulated $W \to e\nu_e$ events to construct a signal template. The control sample is selected by employing looser electron identification criteria based solely on shower shape information and inverting the isolation requirement. In addition, if the event contains a jet reconstructed at EM scale with $E_{\mathrm{T}} > 25$ GeV, the difference between the azimuthal angle of the jet and $p_{\mathrm{T}}^{\mathrm{miss}}$ is required to be greater than $\pi/2$. This condition suppresses events with spurious $p_{\mathrm{T}}^{\mathrm{miss}}$ originating from miscalibration of a jet [54]. The nominal $p_{\mathrm{T}}^{\mathrm{miss}}$ and m_{T} criteria are also applied to the control sample. The background and signal templates are fit to the data as a function of p_{T}^{e} in the signal region after electroweak background subtraction. A result of the fit is shown in Fig. 4. The fit result slightly underestimates the data at $p_{\mathrm{T}}^{e} \simeq 60$ GeV, but this difference is within the total uncertainty of the fit. A significant contribution to this uncertainty comes from the limited number of events available for determining the QCD multi-jet background. The fitting is

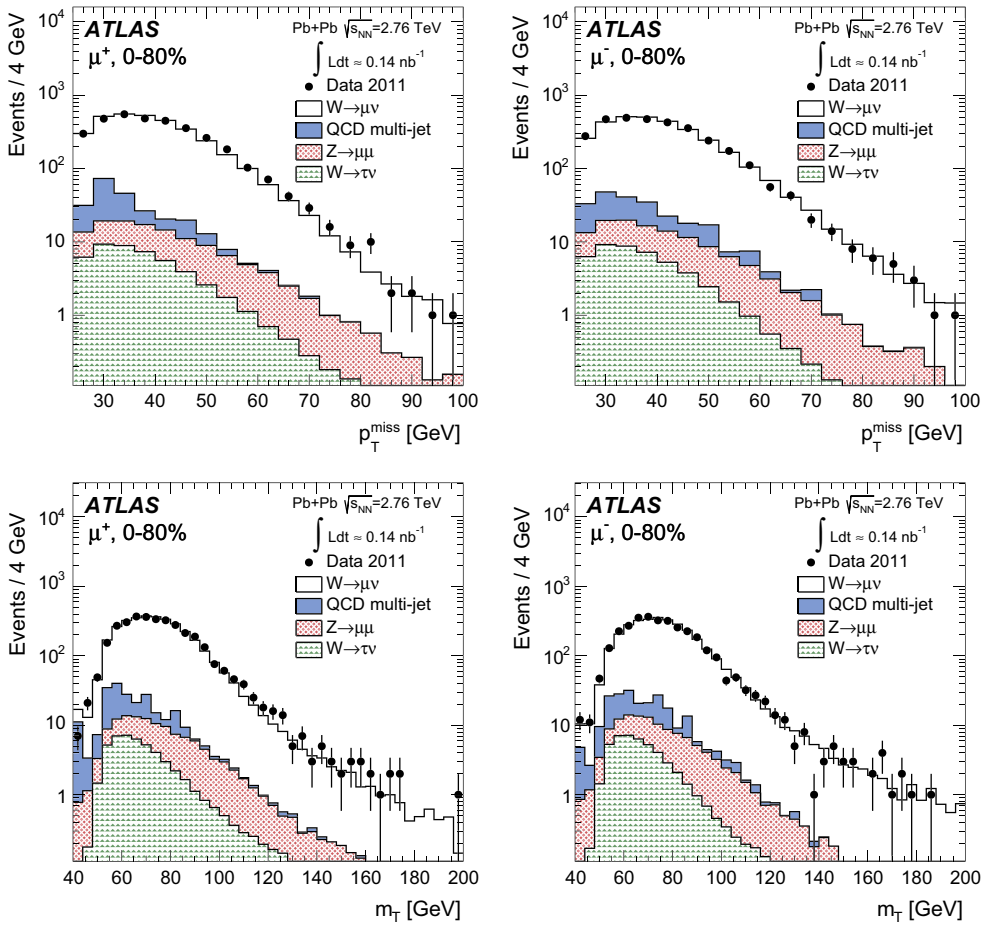

Fig. 3 Measured missing transverse momentum (*top*) and transverse mass (*bottom*) distributions for $W^+ \to \mu^+\nu_\mu$ (*left*) and $W^- \to \mu^-\bar{\nu_\mu}$ (*right*) candidates after applying the complete set of selection requirements in the fiducial region, $p_{\mathrm{T}}^{\mu} > 25$ GeV, $p_{\mathrm{T}}^{\mathrm{miss}} > 25$ GeV, $m_{\mathrm{T}} > 40$ GeV and $0.1 < |\eta_\mu| < 2.4$. The contributions from electroweak and QCD multi-jet processes are normalised according to their expected number of events and added sequentially. The $W \to \mu\nu_\mu$ MC events are normalised to the number of background-subtracted events in the data. The background and signal predictions are added sequentially

performed in all centrality bins and results in a total background estimation of 16.7 % of $W \to e\nu_e$ candidate events in the 0–80 % centrality class. As in the muon channel, this background fraction is charge-independent.

The background from electroweak processes with electrons in the final state is estimated from the MC samples listed in Table 1. The nominal selection criteria of this analysis are imposed on each MC sample. The absolute normalisation is derived from the W and Z POWHEG cross-sections in pp collisions. These cross-sections are scaled by $\langle N_{\mathrm{coll}} \rangle$ in each centrality bin and normalised to the integrated luminosity of the Pb+Pb data sample. This method gives a valid estimate of the electroweak background in this analysis since ATLAS has recently demonstrated that the $Z \to e^+e^-$ yields in Pb+Pb collisions at $\sqrt{s_{\mathrm{NN}}} = 2.76$ TeV are consistent with the pp expectation scaled by $\langle T_{AA} \rangle$ to within 3 % [22]. The $Z \to e^+e^-$ background is the dominant electroweak background in this analysis and amounts to 6.5 % of the total $W \to e\nu_e$ candidate events. The background from $W \to \tau\nu_\tau$ contributes an additional 2.5 %. Electrons from $Z \to \tau\tau$ and $t\bar{t}$ are found to be <0.3 % and <0.1 %, respectively. As with the muon channel, the latter two background sources are considered negligible.

Figure 5 shows the $|\eta_e|$ and p_{T}^{e} distributions for positively and negatively charged electrons after final event selection. Figure 6 presents the event $p_{\mathrm{T}}^{\mathrm{miss}}$ and m_{T} distributions. In each figure, the data are compared to signal and background distributions from MC simulation in the same phase space. The background distributions are normalised to the expected number of events, whereas the signal MC distribution is normalised to the number of background-subtracted events in the data. The background and signal predictions in Figs. 5 and 6 are added sequentially, beginning with the contribution from $W \to \tau\nu_\tau$.